Two-bunch seeding of soft x-ray free electron lasers

E. Schneidmiller[*] and I. Zagorodnov[†]
Deutsches Elektronen-Synchrotron DESY, Notkestr. 85, 22607, Hamburg, Germany

(Received 1 July 2024; accepted 31 October 2024; published 21 November 2024)

Seeded free electron lasers (FELs) demonstrate a good performance and are successfully used in different user experiments in extreme ultraviolet and soft x-ray regimes. In this paper, a simple modification of the seeding scenario is proposed relying on the generation of two closely spaced bunches with very different properties: a low-current seeding bunch and a high-current bunch that amplifies coherent radiation, produced by the seeding bunch. This approach eliminates different limitations and mitigates some harmful effects in the standard scenario. In particular, one can generate very high harmonic numbers with a moderate laser power in a simple high-gain harmonic generation (HGHG) scheme. Alternatively, in case of moderate harmonic numbers, one can strongly reduce the required laser power thus simplifying the design of high repetition rate seeded FELs. An influence of beam dynamics effects (like nonlinearities of the longitudinal phase space of electron beams, coherent synchrotron radiation, longitudinal space charge, geometrical wakefields, and microbunching instabilities) on properties of the output radiation (spectrum broadening, pedestals, and stability) can be to a large extent reduced in the proposed scheme. In this paper, we illustrate the operation of the two-bunch seeding scheme in HGHG configuration with realistic start-to-end simulations for the soft x-ray user facility free electron laser in Hamburg. We show that nearly Fourier-limited multigigawatt pulses can be generated at 4 nm using the present compact design of the undulator system. With several thousand pulses per second, this can be a unique source for photon science.

DOI: 10.1103/PhysRevAccelBeams.27.110703

I. INTRODUCTION

Implementation of seeding schemes in high-gain short-wavelength FELs promises exceptionally bright output radiation with stable properties [1]. There are two main schemes that have been proposed and tested: high-gain harmonic generation (HGHG) [2] and echo-enabled harmonic generation (EEHG) [3].

In case of HGHG, an electron beam is modulated in energy by a laser in a modulator undulator followed by a chicane where the energy modulations are converted into density modulations. The latter are nonlinear, i.e., the electron density contains higher harmonics that produce radiation in the following undulator (FEL amplifier) tuned to one of those harmonics. If this undulator is sufficiently long, the radiation is amplified up to FEL saturation. This scheme is conceptually and technically simple, and it was successfully tested at different facilities and used in routine operation for users [1]. However, there is an intrinsic limitation that does not allow to use this concept at very high harmonic numbers. In order to generate density harmonic number n in the modulator-chicane system, one should impose the energy modulation $\Delta\mathcal{E}$ that is significantly larger than uncorrelated energy spread in the electron beam $\sigma_\mathcal{E}$ [2]:

$$\frac{\Delta\mathcal{E}}{\sigma_\mathcal{E}} > n. \tag{1}$$

One problem with this condition is that strong energy modulations at large harmonic numbers can prevent lasing in the amplifier. A possible method to deal with this issue is the so-called "fresh bunch technique" proposed in [4]. Another problem is that the required laser power (for a given uncorrelated energy spread) scales as the square of harmonic number, $P_L \propto (\Delta\mathcal{E})^2 \propto n^2$, what often makes generation of very high harmonics impractical. A possible approach to reach high harmonic number could be a modified HGHG setup that incorporates the optical klystron effect [5–7] with a subsequent use of the fresh bunch technique [8]. However, this method requires very bright electron beams to reach short wavelengths. Moreover, an additional chicane, required for this scheme, should have a large longitudinal dispersion (characterized by the momentum compaction factor R_{56}), which can contribute to a development of the microbunching instability [9–11].

[*]Contact author: evgeny.schneidmiller@desy.de
[†]Contact author: igor.zagorodnov@desy.de

The key parameter for HGHG scheme, as can be seen from Eq. (1), is the uncorrelated energy spread. It is usually small in injectors of FEL drivers but then it increases proportionally to a peak current in bunch compression systems. High peak current is needed for a successful operation of the FEL amplifier at short wavelengths. This is an intrinsic contradiction of the present operating regimes of the seeded FELs: the same bunch with a high current and a relatively large uncorrelated energy spread is used to generate harmonics in modulator-chicane system, and then to produce the radiation at a harmonic in the amplifier. We propose to separate these functions by generation of two bunches in the accelerator that drives the FEL: a weakly compressed bunch with low current and low energy spread to be used in the modulator-chicane system, and a strongly compressed bunch to amplify the radiation produced by a weakly compressed bunch. The main goal of our studies is to understand if such bunches can be simultaneously produced in a typical accelerator used as FEL driver. We use parameters of accelerator of the first soft x-ray FEL user facility free electron laser in Hamburg (FLASH) [12,13] being upgraded toward high repetition rate seeded FEL facility [14].

Apart from solving the main conceptual problem of seeded FELs, as briefly discussed above, two-bunch approach has additional advantages: improved spectral brightness and stability of FEL radiation, relaxed requirements to laser power (which can be important for high repetition rate FELs), etc. In this paper, we concentrate on HGHG scheme and only briefly discuss EEHG. The EEHG concept is more sophisticated than HGHG, it involves two lasers, two modulators, and two chicanes [3]. Although the condition (1) is not applied to EEHG case, the required energy modulations by lasers are still proportional to uncorrelated energy spread, i.e., EEHG method can also strongly profit from two-bunch concept.

We should note that two-bunch self-seeding of x-ray FELs [15] was proposed in [16,17]. Moreover, experimental demonstration of two-bunch operation of SASE FELs (self-amplified spontaneous emission free electron lasers [18]) was described in [19–21], while the results of experiments with two bunches in seeded FELs were published in [22,23]. In this paper, we propose a new application of two-bunch FEL operation promising a generation of high-quality radiation pulses at short wavelengths.

II. THE CONCEPT OF TWO-BUNCH SEEDING

Conceptual scheme of two-bunch seeding of a short-wavelength FEL is shown in Fig. 1. The scheme looks similar to that proposed in [4] with the difference that we want to use two bunches with different properties. Therefore, we start the discussion with the generation of two bunches in an accelerator system. A typical driver of a high-gain short-wavelength FEL consists of a laser-driven rf gun, rf accelerating sections, bunch compressors, and, eventually, a laser heater. The only hardware modification required for operation of two-bunch scheme is the installation in a laser system of a split-and-delay unit with an attenuator in one of the branches. Alternatively, two lasers can be used as in the case of FLASH. Two bunches with, generally speaking, different charges and controllable time delay are extracted from the cathode of the rf gun and are then compressed in a different way since they propagate in different fields of rf cavities. They arrive at the entrance of seeded FEL such that the low-current bunch (which we will call seeding bunch or S-bunch) is behind the high-current bunch (amplifying bunch or A-bunch). The S-bunch with low uncorrelated energy spread is modulated by a seed laser with a subsequent conversion of energy modulation into density modulation (HGHG scheme) or is being manipulated in a more complex way with the help of two lasers (EEHG). The S-bunch, containing higher harmonics of the laser in density distribution, then produces coherent radiation at a harmonic in a relatively short undulator (this is often referred to as coherent harmonic generation or CHG). In the following delay chicane, both bunches are delayed with respect to the radiation pulse, which is parked on the A-bunch and is amplified to saturation in a long amplifier. The bunching in the S-bunch is smeared in the chicane, so that this bunch can only produce SASE in the amplifier but due to its low current the gain is low, and the generated

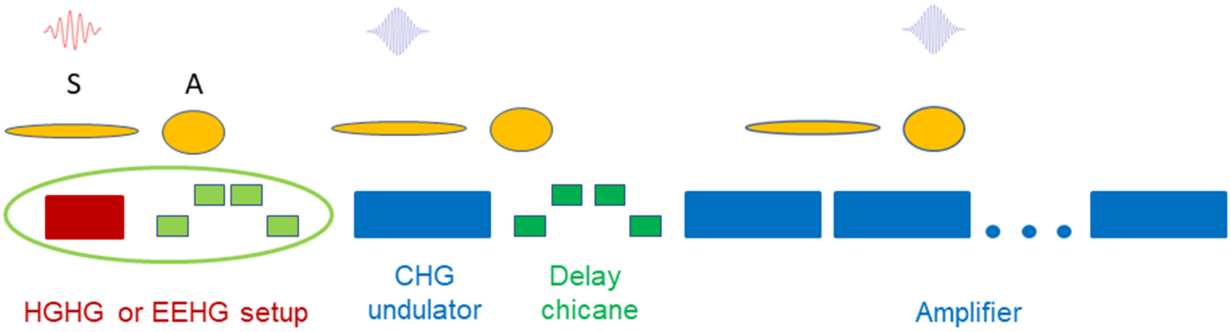

FIG. 1. Conceptual representation of two-bunch seeding scheme. Seeding and amplifying bunches are marked with "S" and "A," respectively.

background is negligible (the same refers to the radiation produced by A-bunch in a short CHG undulator). Below in this section, we will briefly discuss different aspects of the two-bunch scheme concerning the formation of bunches in the accelerator and FEL operation.

A. Beam dynamics

1. The photoinjector

The photoinjector laser system can be simply upgraded by adding a split-and-delay unit, for example, of interferometer type (with adjustable delay and attenuator). Thus, two pulses with the same length but different intensities and a controllable delay are generated. Some FEL facilities like FLASH [12] and European XFEL [24] are equipped with two photoinjector lasers allowing to produce two pulses with different properties and controllable delay. The cathode of the rf gun is illuminated by two pulses, and two electron bunches with equal or different charges are produced. The rf phases of two pulses can differ significantly what potentially might be a challenge because emittances and Twiss parameters of these bunches can be essentially different. Transverse mismatch, generated in the injector and later in the linac, can be controlled and minimized independently for both bunches as explained below.

2. Bunch compression

Typical bunch compression system consists of one or two chicanes operated at different energies. To linearize compression process, a high harmonic rf cavity is typically used (third harmonic in case of FLASH). When optimizing compression of two bunches, we came to the conclusion that it is better to use overcompression regime, see the details below in this paper. In particular, it means that the two bunches change their relative positions: S-bunch leaves the gun first but arrives at the FEL setup last. Since S-bunch is only weakly compressed, its properties are expected to be stable, and this will guarantee high spectral stability of the output FEL radiation.

3. Collective effects

Operation of seeding schemes is sensitive to the collective effects in the beam formation and transport systems. Collective effects like space charge, coherent synchrotron radiation (CSR), and geometrical wakefields in a linac lead to a degradation of beam quality, and the degradation is more significant for strongly compressed bunches. In our simulations, the most important collective effects are properly included but we do not see any essential deterioration of the longitudinal phase space of the S-bunch because it is weakly compressed. At the same time, the action of A-bunch on S-bunch is weak, as we see in numerical simulations. As it will be discussed in more detail below, the properties of the longitudinal phase space (LPS) of the S-bunch define the spectral quality of the output radiation so that it can be kept almost ideal.

4. Mismatch control

One of the possible issues with the proposed scheme might be a strong difference in properties of the transverse phase spaces (characterized by Twiss parameters) of the two bunches. The reason is that they are formed and evolve under the action of very different transverse forces from rf fields as well as from collective fields (mainly space charge), especially in the injector. The problem is solved by introducing two additional matching points in the machine (assuming that the A-bunch is matched in the linac). The first one is in front of the FEL setup where the S-bunch is matched. The second one, for the A-bunch, is between the CHG undulator and the amplifier where the matching can be done by quadrupoles before and after the delay chicane. Since bunches can be switched on and off independently, one can observe and analyze the image of the relevant bunch only. Fine matching can be done empirically while optimizing FEL performance.

B. FEL operation

1. HGHG and EEHG

There is a consensus among FEL physicists that seeding at high harmonic numbers should be done with the EEHG scheme. Indeed, it does not have the limitation (1), so that for a given energy spread one can go to a much higher harmonic number than in the case of a single-stage HGHG. (Indeed, in the latter case, it is hard to overcome harmonic number 20 as shown in [25].) At the same time, EEHG requires a chicane with a relatively large R_{56} in the first stage, which can create serious problems. The most significant issue is that appearance of this chicane results in one more amplification cascade for the microbunching instability [26]. Another problem is a distortion of the longitudinal phase space in this chicane due to coherent synchrotron radiation (CSR) that can result in a reduced bunching factor [27]. In addition, intrabeam scattering effects can deteriorate the process of generation of a large bunching factor at high harmonic numbers. The two-bunch seeding concept mitigates the mentioned issues due to a low current of the S-bunch.

Moreover, the concept makes it possible to generate high harmonics in a relatively simple HGHG configuration. In this case, the required R_{56} is typically by two orders of magnitude smaller than in the case of the first stage of EEHG. Thus, such effects as additional microbunching instability gain or CSR in dipoles of the chicane do not play a significant role anymore. In this paper, we concentrate on HGHG case leaving EEHG for future studies. Below, we would like to qualitatively discuss potential advantages of the two-bunch seeding even if we do not aim at studying sensitivity and stability aspects in this paper.

2. Spectral quality and stability

Spectral quality of seeding schemes is sensitive to the longitudinal phase space of electron bunches. In case of the standard HGHG scheme, the beam is modulated by a laser in the modulator undulator, and a nonlinear transformation of LPS, leading to the appearance of high harmonics of the laser in electron density, occurs in the chicane. Since LPS is never ideal, its imperfections are embedded in bunching at higher harmonics and lead to a degradation of spectral quality of the radiation produced in the amplifier. In particular, a linear energy chirp results in a shift of central wavelength. It is not critical by itself but may lead to shot-to-shot variation of the wavelength if the compression is not stable. Nonlinear chirp leads to a spectral broadening, moreover the jitter of the central wavelength can also occur if there is an arrival time jitter between the bunch and the laser pulse [28]. High-frequency modulations of the electron bunch due to the microbunching instability can lead to the generation of sidebands, a pedestal, etc. Note that all these effects are much weaker in the amplifier because its R_{56} is much smaller than that of the chicane.

In the case of two-bunch seeding, a long low-current bunch is used for harmonic conversion in the modulator-chicane system, and the spectral quality and stability are much less affected. There is, in general, a linear chirp leading to the wavelength shift but this chirp is very stable due to a reduced compression factor. Nonlinearities of the LPS of S-bunch are relatively small, i.e., one should expect neither significant spectrum broadening nor the jitter of the central wavelength. Microbunching instability is also expected to play a less significant role in the case of low-current bunch. High-current A-bunch can be stronger distorted due to collective affects and can be less stable due to a stronger bunch compression but, as it was just mentioned, the deteriorating effects in the amplifier are much weaker.

3. Debunching in drifts and undulators

The modulated electron beam after the modulator-chicane system can relatively quickly lose bunching at high harmonics due to nonlinear space charge forces in the drifts and in the undulators [29]. Recent experimental studies [30] in a standard HGHG setup show that the effect can lead to a significant debunching on a relatively short distances if the beam current is high. In case of two-bunch seeding, the current of S-bunch is low, and the CHG undulator is not long, so that these effects are not expected to play any significant role.

4. High harmonic numbers or a reduced laser power

Since the uncorrelated energy spread of the S-bunch is relatively small, according to the condition (1), we can either go for a high harmonic number or strongly reduce the required laser power in case of moderate harmonic numbers. If, for example, the energy spread in the S-bunch is reduced by an order of magnitude with respect to a standard case, the laser peak power can then be smaller by two orders. The laser power reduction can also be achieved with the optical klystron approach [6,7] (even though the quality of the output radiation might have to be compromised due to an additional strong chicane). Here, we would like to mention that both approaches, two-bunch seeding and optical klystron, can be combined thus leading to enormous reduction of the required laser power and making high repetition rate CW seeded FELs possible.

In this paper, we do not consider the laser power reduction and concentrate on the generation of high harmonic numbers.

III. SIMULATIONS OF BEAM DYNAMICS IN FLASH ACCELERATOR

Beam dynamics of two bunches, used for different purposes, was previously studied in [20,31,32]. We perform numerical simulations of beam dynamics in FLASH accelerator with the goal to find a good solution for our two-bunch seeding scheme.

FLASH [12] is the first free-electron laser for XUV and soft x-ray radiation. It covers a wavelength range from 4 to about 90 nm with GW peak power and pulse durations between a few fs and 200 fs. The electron bunches with maximum energy of 1.35 GeV are distributed between the two branches, FLASH1 and FLASH2 [13]. The facility is based on the superconducting accelerator, which allows to operate in a "burst mode" with long pulse trains (several hundred pulses) at 10 Hz repetition rate. Presently, the

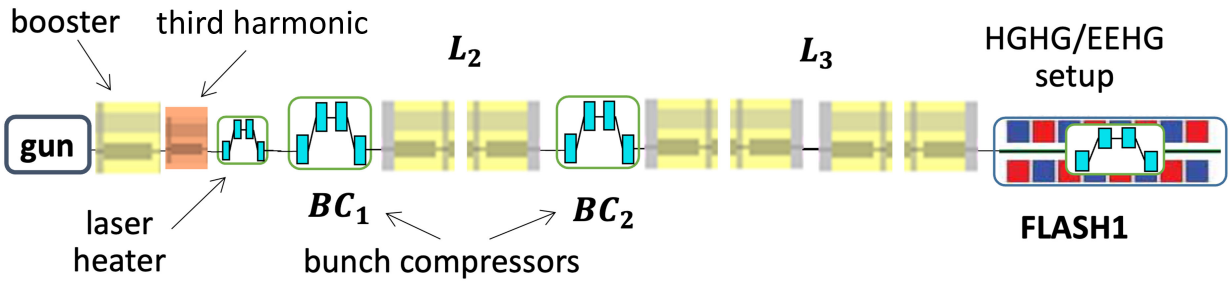

FIG. 2. The layout of FLASH1.

TABLE I. Maximal accelerating voltage in rf sections.

Section name	Booster	Third harmonic	L_2	L_3
Maximal voltage (MV)	170	22.5	440	800

TABLE II. Range of momentum compaction factors in the bunch compressors.

Section name	BC_1	BC_2
$\lvert R_{56}\rvert$ (mm)	120–250	0–105

facility is being upgraded toward high repetition rate seeding in the FLASH1 branch [14].

The layout of facility with FLASH1 branch is shown in Fig. 2. In order to compress the beam to a high peak current, the electron beam line incorporates two horizontal bunch compressors of C type.

The maximal accelerating voltages at different sections of the accelerator (as it was assumed in the simulations) are listed in Table I. The ranges for the compression compaction factors are presented in Table II.

The linear optics [33] is shown in Fig. 3. It starts after the rf gun at the position $z = 2.6$ m from the gun cathode. The position $z = 2.6$ m corresponds to the beginning of the booster rf module with eight TESLA superconducting cavities (see Fig. 2). The lattice has additional dispersive element (injection chicane [34] of the laser heater [35]), which has to be taken into account when looking for working points with a desired global compression. In the current design, the momentum compaction factor R_{56}^{LH} of the laser heater is equal to -2.5 mm. The second-order optics gives the second-order momentum compaction factor of the laser heater T_{566}^{LH} equal to 3.7 mm [see Eq. (7) for the definition of R_{56} and T_{566}]. We will use these values in order to correct the momentum compaction factors of the first compression stage in the simple analytical model described below.

The electron bunches, each with the charge of 250 pC, are produced by shaped laser pulses in the rf gun. The parameters used in the gun simulations for two bunches are listed in Table III. The rf phase is given relative to the phase of maximal mean momentum.

The simulations are done with code ASTRA [36]. In our simulations, we use 2×10^6 macroparticles per bunch. The slice parameters and the phase space projections at the distance 2.6 m from the cathode are shown in Fig. 4. In order to calculate the slice parameters, we have used 5e3 particles per slice. The "emittance" means in this paper the rms normalized emittance.

In order to describe the longitudinal beam, dynamics inside the bunch during the compression and acceleration let us introduce several coordinate systems. As a starting point, we consider the two bunches of electrons after the rf-gun at position $z = 2.6$ m. The relative coordinate along the bunches will be noted as s. It has an origin at the position of the peak current at the A-bunch and increases in the direction of the bunch motion: the head of the bunch has a positive value of s, the tail has a negative one. The peak current in the S-bunch is at the position $s = 10$ mm.

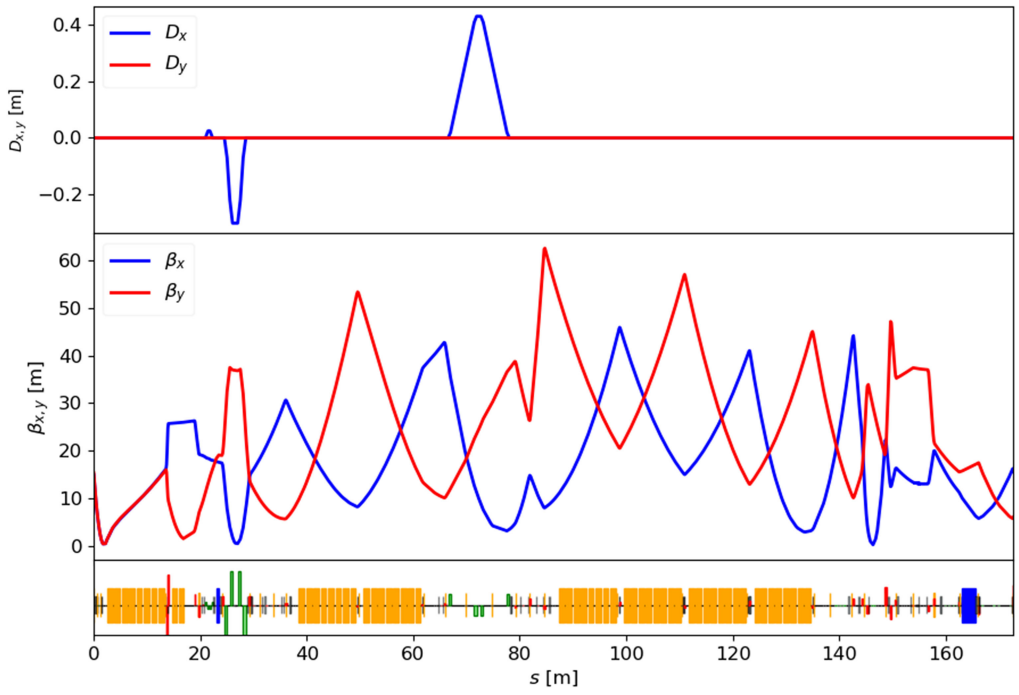

FIG. 3. The design optics of FLASH1. The bottom plot presents an outline of different elements: quadrupoles (in red), dipoles (in green), and rf modules (in orange).

TABLE III. The injector parameters.

Subsection	Parameter	A-bunch	S-bunch
Laser	rms length (ps)	4	4
	Apperture diameter (mm)	1.15	1.15
rf cavity	Frequency (GHz)	1.3	1.3
	Maximal field on cathode (MV/m)	45	45
	Relative phase (deg)	10	10
Solenoid	Magnetic field (T)	0.172	0.172

The longitudinal phase space of A-bunch can be approximated locally by the third order polynomial

$$E_0^A(s) = E_0^{\mathrm{ref},A}(1 + \zeta_1^A s + \zeta_2^A s^2 + \zeta_3^A s^3), \tag{2}$$

with the coefficients from the first column of Table IV. The longitudinal phase space of S-bunch can be approximated locally by the third order polynomial

$$E_0^S(s) = E_0^{\mathrm{ref},S}(1 + \zeta_1^S(s - 0.01\ \mathrm{m}) + \zeta_2^S(s - 0.01\ \mathrm{m})^2 + \zeta_3^S(s - 0.01\ \mathrm{m})^3), \tag{3}$$

with the coefficients from the second column of Table IV.

Hence after the rf gun the mean slice energy can be approximated by step-wise function

$$E_0(s) = \begin{cases} E_0^A(s), & s \le 0.0055\ \mathrm{m}, \\ E_0^S(s), & s > 0.0055\ \mathrm{m}, \end{cases} \tag{4}$$

shown by the dotted curve in Fig. 4.

For the fixed reference energy E_0^{ref}, we introduce the relative energy deviation coordinate $\delta_0(s) = (E(s) - E_0^{\mathrm{ref}})/E_0^{\mathrm{ref}}$.

Let us consider the transformation of the longitudinal phase space distribution in a multistage bunch compression and accelerating system shown in Fig. 2. The system has two bunch compressors $\{BC_1, BC_2\}$ and several accelerating sections $\{L_1, L_2, L_3\}$. The injector section L_1 includes the booster and the third harmonic module.

In order to describe the longitudinal beam dynamics, we introduce several additional reference points to already described one (after the rf gun). The longitudinal coordinate after bunch compressor number i will be denoted as s_i, the energy coordinate at the position immediately after the bunch compressor will be denoted as δ_i. The reference particle is always at the position s_i^{ref}. The coordinate s (position in the bunch after the rf gun) will be used as an independent coordinate. All other functions depend on it. For example, the function $s_i(s)$ means that the particle with the initial position s (in the bunch after the rf gun) has the position s_i after bunch compressor BC_i. In the following, we omit the dependence on coordinate s in the notation.

For relativistic electrons, interacting with sinusoidally time varying field, the energy gain of the electron is

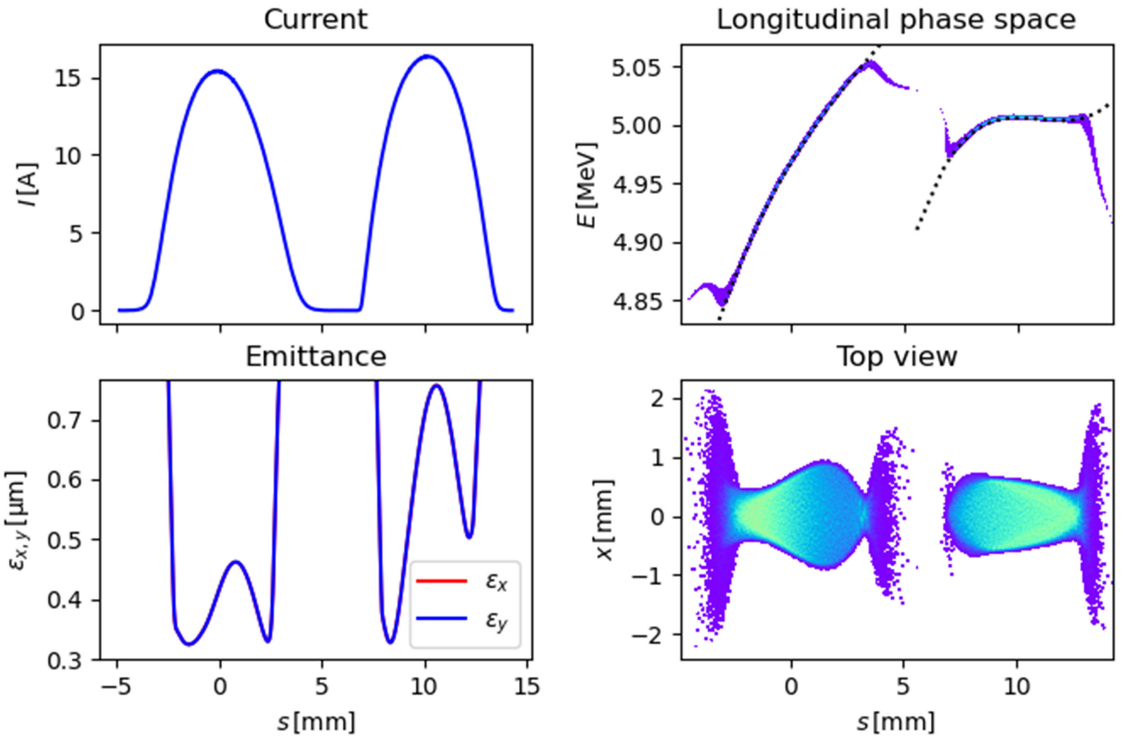

FIG. 4. The properties of the two bunches at distance $z = 2.6$ m from the cathode of rf gun. The dotted line in the longitudinal phase space corresponds to Eq. (4).

TABLE IV. The longitudinal phase space bunch parameters after the rf gun at distance $z = 2.6$ m from cathode.

Parameter	A-bunch	S-bunch
E_0^{ref} (MeV)	4.97	5.01
ζ_1 (1/m)	6.42	−0.14
ζ_2 (1/m/m)	−420	−390
ζ_3 (1/m/m/m)	38 590	140 748

proportional to the cosine of the phase angle between its position and the position of maximum energy gain. Hence, the energy changes in the accelerating sections can be approximated as

$$\Delta E_{11} = eV_{11}\cos(ks+\varphi_{11}), \quad \Delta E_{13} = eV_{13}\cos(3ks+\varphi_{13}),$$
$$\Delta E_2 = eV_2\cos(ks+\varphi_2), \tag{5}$$

where e is the electron charge, φ_{11}, V_{11} are a phase and an on-crest voltage of the booster, φ_{13}, V_{13} are a phase and an on-crest voltage of the third harmonic module, φ_2, V_2 are a phase and an on-crest voltage of accelerating section L_2, and k is a wave number.

The relative energy deviations in the reference points after the bunch compressors read

$$\delta_1 = \frac{(1+\delta_0)E_0^{\mathrm{ref}} + \Delta E_{11} + \Delta E_{13}}{E_1^{\mathrm{ref}}} - 1,$$
$$\delta_2 = \frac{(1+\delta_1)E_1^{\mathrm{ref}} + \Delta E_2}{E_2^{\mathrm{ref}}} - 1. \tag{6}$$

The transformation of the longitudinal coordinate in compressor number i can be approximated by the expression

TABLE V. The longitudinal dynamics parameters.

E_1^{ref} (MeV)	$(R_{56})_1$ (mm)	C_1	E_2^{ref} (MeV)	$(R_{56})_2$ (mm)	C_2	C_2' (1/m)	C_2'' (1/m/m)
130	−122	3	550	−104	−130	0	0

$$s_i = s_{i-1} - (R_{56i}\delta_i + T_{566i}\delta_i^2 + U_{5666i}\delta_i^3), \quad i = 1,2, \tag{7}$$

where R_{56i}, T_{566i}, and U_{5666i} are the first, the second, and the third order momentum compaction factors of the corresponding chicanes. Equations (4)–(7) present a simple nonlinear model of multistage bunch compression system.

For the fixed values of rf parameters and momentum compaction factors, we define the compression functions in each bunch compressor:

$$C_i(s) = \frac{1}{Z_i(s)}, \qquad Z_i(s) = \frac{\partial s_i(s)}{\partial s}, \quad i = 1,2.$$

The global compression function $C_2(s)$ presents the compression after compressor BC_2, which is obtained for the particles in neighborhood of position s (the position in the bunch after the rf gun). For example, if we would like to increase the peak current by factor 50 at the position of the reference particle, then $C_2(s^{\mathrm{ref}}) = 50$. In other words, function $C_2(s)$ describes the increase of the current in the slice with initial position s.

The energies at the beam compressors are fixed by design studies and are listed in Table V. The global compression C_2 comes from the requirement on the peak current value of 2 kA.

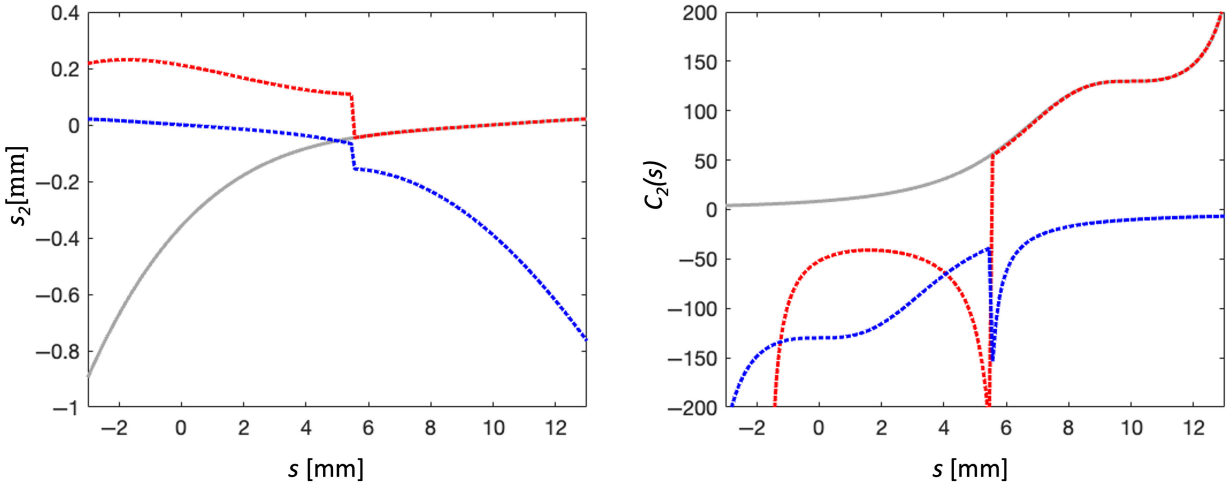

FIG. 5. The position (on the left) and the compression (on the right) curves of the longitudinal dynamics without collective effects. The gray solid curve describes the position (on the left plot) and the compression (on the right plot) for the ideal beam without energy spread. The dashed curves present the position and the compression for the longitudinal phase space approximated by Eq. (4). The red curves correspond to the hypothetical situation when A-bunch leaves the gun first. The blue curves correspond to the simulated case, when the S-bunch leaves the gun first and then the bunches exchange their relative positions during the bunch compression.

TABLE VI. The rf parameters.

	V_{11} (MV)	φ_{11} (deg)	V_{13} (MV)	φ_{13} (deg)	V_2 (MV)	φ_2 (deg)	V_3 (MV)	φ_3 (deg)
Analytical	146.4	5.66	21.0	168.53	436.8	15.95	800	0
With self-fields	144.8	−2.35	22.5	150.42	438.8	16.23	800	0

The first and the second derivatives of the global compression are special parameters that allow to tune the flatness and the symmetry of the current profile. We put them to zeros. It means that we would like to have a flat current profile at the vicinity of the reference position.

The introduced one dimensional model of the longitudinal beam dynamics neglects the collective effects and the velocity bunching. In order to find the rf parameters of the accelerating modules, we use the analytical solution published in [37].

Let us assume first that the lasing bunch is the first bunch at the position $s^{\mathrm{ref}} = 10$ mm. If we assume additionally that the both bunches have no energy chirp and the longitudinal phase space can be approximated by a constant line $E_0(s) = E_0^{\mathrm{ref},S} = 5.01$ MeV then the both bunches can be smoothly compressed according to the compression curve shown by the solid gray line in Fig. 5. The first bunch at the reference position $s^{\mathrm{ref}} = 10$ mm is compressed by factor $C_2(s_{\mathrm{ref}}) = 130$. The second bunch at the position $s = 0$ mm is compressed by the low factor $C_2(0) = 8.4$. The bunches arrive to the end of the linac at the same order as they have been emitted from the gun. Unfortunately, the second bunch has not flat longitudinal phase space, and for the "real" longitudinal phase space approximated by Eq. (4), the compression curve is different. It is shown by dotted red curve in Fig. 5. It can be seen that the second bunch is overcompressed: $C_2(0) = -52$. In the particle tracking simulations, the second bunch arrives as the first to the end of the linac. Hence at the scenario of the flat compression $[C_2(s^{\mathrm{ref}})' = 0, C_2(s^{\mathrm{ref}})'' = 0]$, the second bunch cannot be used as a seed.

In order to use the first bunch at the position $s^{\mathrm{ref}} = 10$ mm as a seed, we should to work in the overcompression scenario that changes the order of the bunches after BC_2. If we require that the second bunch at the position $s^{\mathrm{ref}} = 0$ mm is overcompressed with the compression factor $C_2(0) = -130$, then the compression curve has the form shown by the dotted blue line in Fig. 5. The first bunch is overcompressed by factor $C_2(0.01\ \mathrm{m}) = -10.3$ and the bunches arrive in the reversed order to the end of the linac. The rf parameters for the last curve are listed in the first row of Table VI.

The above results are confirmed with the particle tracking in Ocelot with the collective effects included.

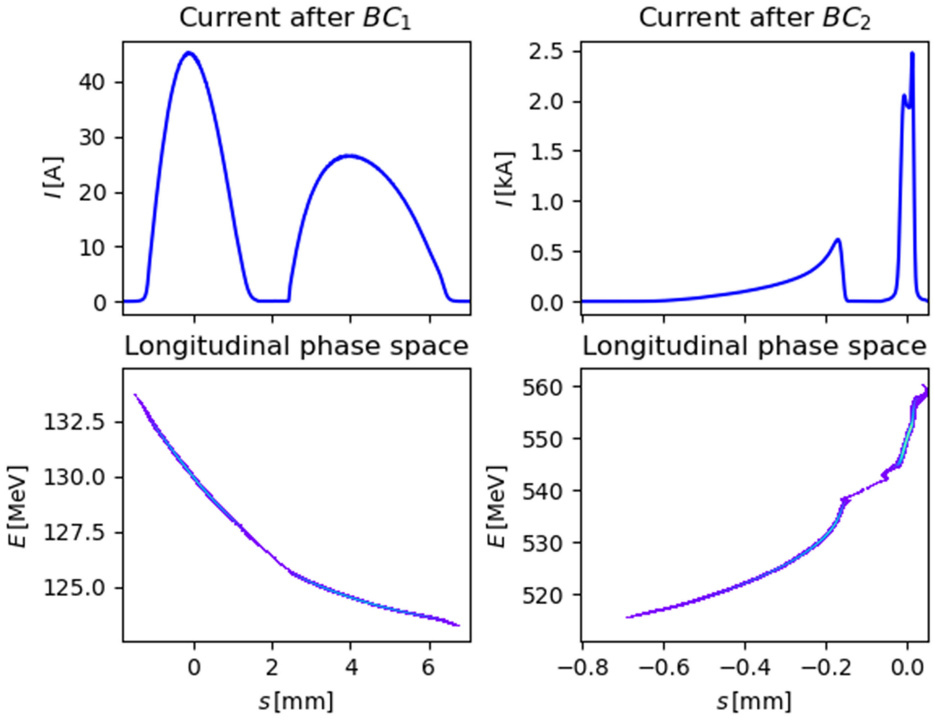

FIG. 6. The current and the longitudinal phase space after bunch compressor BC_1 (on the left) and after bunch compressor BC_2 (on the right).

The rf parameters for this case are listed in the second row of Table VI.

Figure 6 presents the current profiles and the longitudinal profiles of the two bunches after the bunch compressors. It can be seen that after the last compressor BC_2, the bunches change their order and both of them go through the overcompresion.

The physical models and the numerical algorithms of code Ocelot [38] are described shortly in Appendix B of paper [39]. The numerical modeling of the accelerator beam dynamics presented in this paper includes the wake functions of the accelerating modules in the form described in [40]. We have tested with the direct numerical solution of Maxwell equations [41] that this form of the wake functions describes accurately the wakefields in the second bunch as well.

Figure 7 shows the slice parameters of the S-bunch before the modulator (on the left) and of the A-bunch before the amplifier (on the right). The slice parameters of each bunch are shown for the simulation window of 60 μm used in the FEL simulations described below. The peak current of the A-bunch is reduced by approximately 15% in the delay chicane before the amplifier due to the strong energy chirp in the A-bunch. One can notice a relatively small uncorrelated energy spread of S-bunch, about 10 keV at the current of 100 A. The longitudinal brightness of an electron beam depends on different effects, is different at different facilities, and is difficult to reliably predict in simulations. However, we can refer to the measurements at FLASH when the energy spread was below 100 keV at the peak current of 1 kA [42], i.e., the same longitudinal brightness as in our simulations was measured. Moreover,

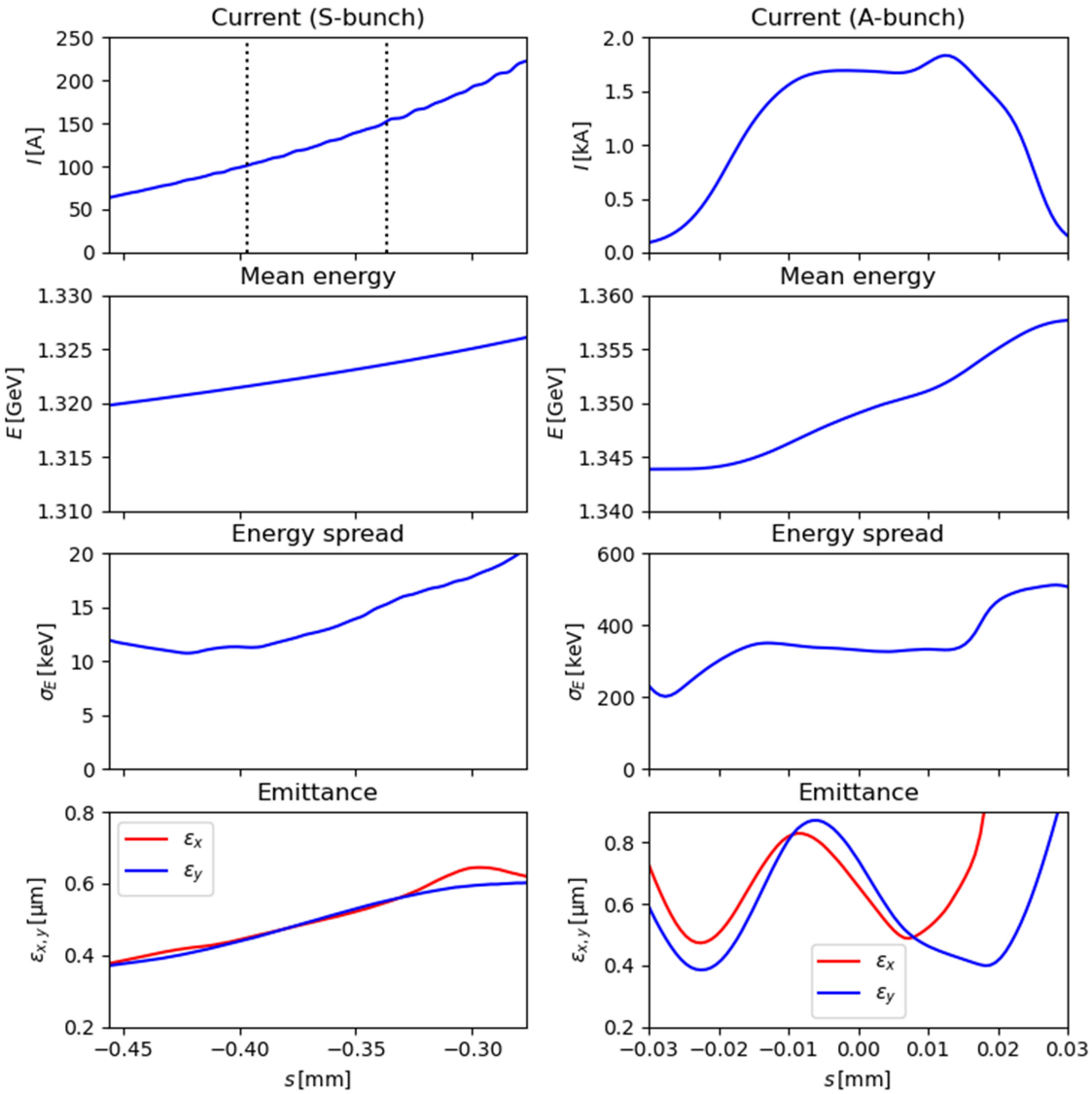

FIG. 7. The current, the mean slice energy, the slice energy spread, and the slice emittance of the seed bunch before the modulator (on the left) and of the lasing bunch before the amplifier (on the right). The dotted lines on the left current plot outline the simulation window used in the FEL modeling.

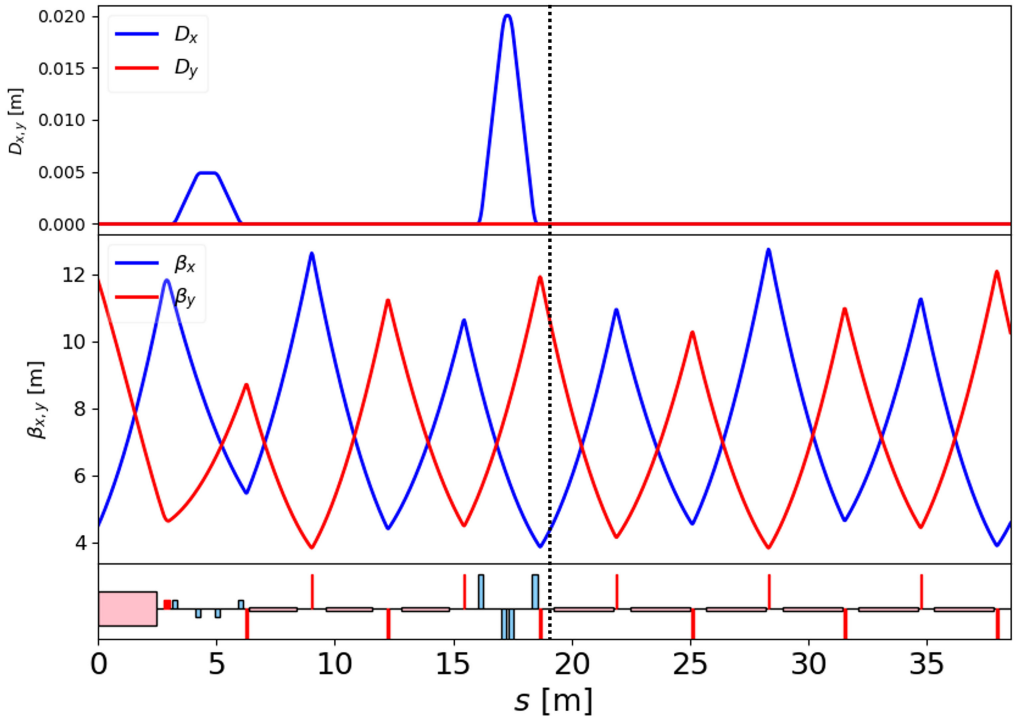

FIG. 8. The design optics of the seeding setup. The bottom plot presents an outline of different elements: quadrupoles (in red), dipoles (in green), and undulators (in blue). The dotted vertical line shows the rematching position for the lasing bunch.

we checked that our scheme works even if the energy spread is significantly larger, see simulations below.

IV. FEL SIMULATIONS

The FEL simulations are carried out with the code Genesis-1.3-Version4 [43] in the optics shown in Fig. 8. The S-bunch is matched to the entrance of the setup. The same transformation was applied for both bunches. It resulted in considerable optics mismatch for A-bunch. The mismatched A-bunch was tracked in Ocelot to the position before the amplifier shown by the dotted line in Fig. 8 and matched to the optics. The Genesis FEL simulations are done with S-bunch up to this position and with A-bunch after it. Hence we assume that it is possible to develop a matching section that will match the A-bunch to the optics of the amplifier section, the details we leave for future studies. The simulations are done with real number of particles, and shot noise is properly included.

The FEL setup is close to the design of the new undulator line of FLASH1. The only simplification we did in simulations is the removal of a small chicane in the amplifier part (it will be installed later but will not be used in our scheme). The delay chicane between CHG undulator and the amplifier will also not be installed initially. Thus the two-bunch seeding will be enabled only after installation of that chicane.

The main parameters used in FEL simulations are presented in Table VII. The CHG undulator is planar and consists of three segments followed by the delay chicane. The amplifier is place behind the chicane and consists of six segments with variable polarization. We simulate two cases: linear and circular polarization of the amplifier undulator. In the latter case, only a half of the radiation power from CHG undulator is coupled to the amplifier (linearly polarized beam can be decomposed into left and right circularly polarized beams), so that we introduce the reduction by a factor of two in our simulations.

TABLE VII. The parameters of FEL simulations.

Subsystem	Parameter	Value
Laser	Laser pulse duration (FWHM) (fs)	33
	Laser wavelength (nm)	300
	Laser power (MW)	100
Modulator	Undulator period (cm)	8.26
	Number of periods	30
	Undulator parameter K_{rms}	6.9117
Chicane	R56 (μm)	52
Radiator	Number of modules	3
	Undulator period (cm)	3.15
	Number of periods in one module	63
	Undulator parameter K_{rms}	0.8400
Delay chicane	R56 (μm)	740
Amplifier	Number of modules	6
	Undulator period (cm)	3.5
	Number of periods in one module	72
	Undulator parameter K_{rms}	0.7725

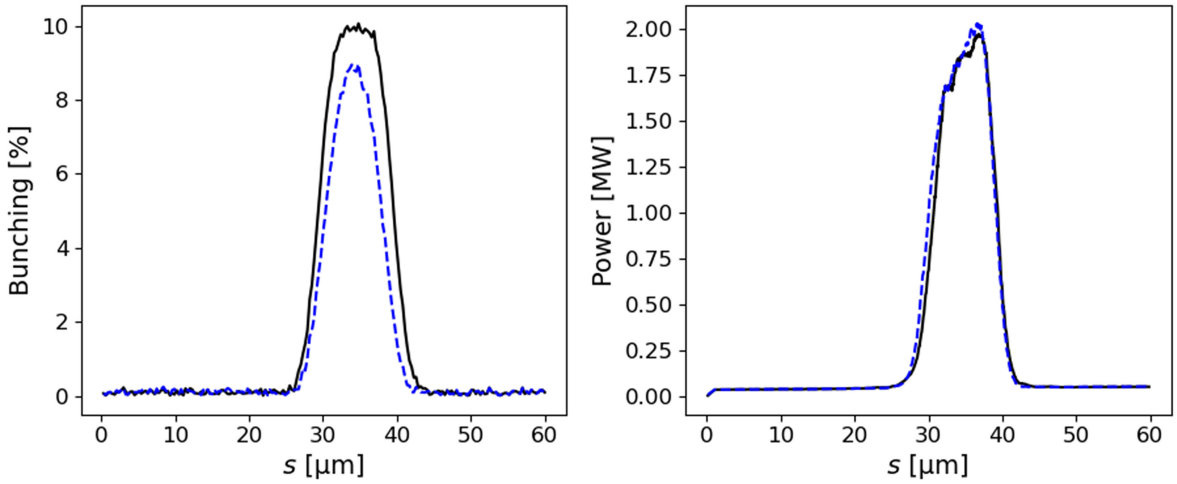

FIG. 9. The left plot shows the bunching factor at the seeding bunch after the CHG radiator. The right plot presents the FEL power profile after the radiator. The black curves are simulated for beam parameters from Fig. 7, while the dashed blue curves are simulated for the case when the uncorrelated energy spread of the S-bunch is artificially increased to 30 keV.

The laser pulse is parked on the part of the S-bunch that can be seen in Fig. 7. For a given power of the laser pulses (100 MW), we optimize the R_{56} of the chicane. The bunching factor after the modulator-chicane system is shown in Fig. 9. One can notice a relatively high value of the bunching factor (nearly 10% at the 75th harmonic of the laser despite its moderate peak power). This is possible due to the small uncorrelated energy spread in the corresponding part of S-bunch, about 10 keV. The radiation pulse at the wavelength of 4 nm, produced in CHG undulator, is also shown in Fig. 9. The bunching and the power are plotted versus longitudinal coordinate as they are extracted from Genesis simulations, one can easily convert it to time coordinate. Note that during the simulations, we optimize the K-value of the CHG undulator.

To prove that our results do not critically depend on the uncorrelated energy spread, we artificially increased it to 30 keV in the part of the S-bunch, shown in Fig. 7. Obviously, in this case, one needs a higher laser power and a lower R_{56} of the chicane. By tweaking these two parameters, we could get a similar distribution of power at the exit of CHG radiator (shown as blue dashed curve in Fig. 9). The laser power in this simulation was 650 MW, and the R_{56} was 15.4 μm. The bunching in Fig. 9 is somewhat lower because dynamics in the radiator is slightly different due to larger energy modulations.

After the CHG undulator the soft x-ray radiation pulse is propagated in a drift space (diffraction is properly included in the simulations), and then it is parked on the part of the A-bunch shown in Fig. 9. The delay in the chicane is about 0.37 mm (slightly larger than 1 ps). The corresponding $R_{56} = 0.74$ mm is sufficient for a complete smearing of the modulations in S-bunch at 4 nm. Moreover, its current is too low to have any significant FEL gain in the amplifier.

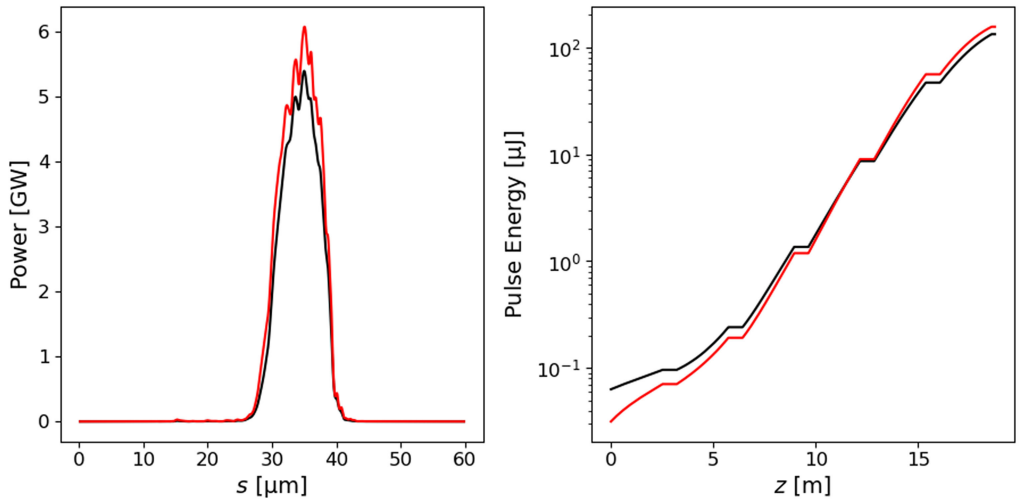

FIG. 10. The left plot shows the output FEL power profiles of planar (black curve) and helical (red curve) undulators. The right plot presents the gain curves of planar (black curve) and helical (red curve) undulators.

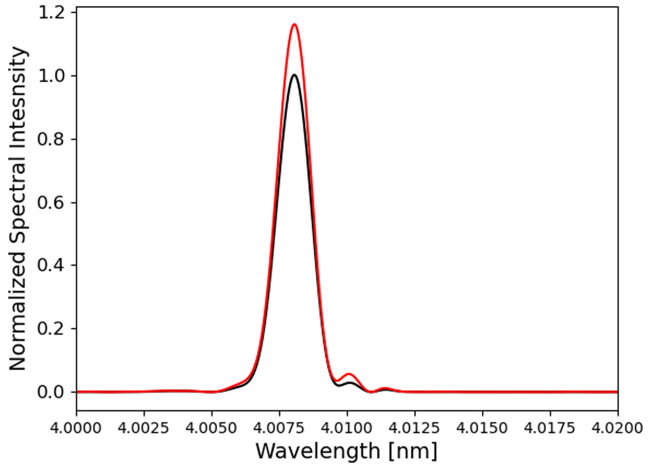

FIG. 11. Output FEL spectra of planar (black curve) and helical (red curve) undulators.

The radiation pulses produced by the A-bunch after six segments of the amplifier undulator for linear and circular polarization cases are shown in Fig. 10 along with the corresponding gain curves. Pulses energies at the undulator end are about 150 μJ, pulse durations about 25 fs. Despite in the circularly polarized case the effective input power is lower, the FEL gain and the output power are somewhat higher due to a better coupling between the electron motion and the electromagnetic field [18]. Note that we optimized K-value of the amplifier undulator to maximize the FEL power. If the undulator was longer, a higher radiation power could be produced with some postsaturation taper. However, even in the simulated case with six undulator segments we can observe multigigawatt peak power thanks to the high peak current of the A-bunch.

Output radiation spectra for the cases of linearly and circularly polarized radiation are presented in Fig. 11. Despite the slight distortions, one can notice a relatively high quality of spectra at the high harmonic number considered in this paper. The relative spectrum width is about 3.4×10^{-4} (FWHM), and the time-bandwidth product exceeds Fourier limit for a Gaussian pulse by only 40%.

V. DISCUSSION

As it was mentioned above, in a standard HGHG configuration, it is difficult to exceed harmonic number 20 [25]. In this paper, we simulated two-bunch seeding case with harmonic number equal to 75, and this is still to be demonstrated experimentally. The question arises what would be the limit of this technique in terms of harmonic number $n_{\max}$ and the shortest wavelength. Let us briefly discuss different effects and limitations using the simulated beam parameters as a reference (and assuming that we can change parameters of the undulators). We do not consider practical limitations as, for example, available laser power or its stability but rather concentrate on physical effects in the proposed scheme.

One limitation is easy to formulate if we want only one harmonic of the laser to be amplified. If we are interested in harmonic n, then the relative frequency difference between adjacent harmonics $\delta\omega/\omega_0 \simeq 1/n$. The neighboring harmonics are filtered out in the CHG radiator and in the amplifier so that we need to have a sufficiently small bandwidth of the product of spectral curves. If we do not want to restrict ourselves with the number of periods in the CHG radiator (which can be quite short, in general), then we assume that the filtering is mainly provided by the amplifier of which rms relative bandwidth can be estimated as $\sigma_\omega/\omega_0 \simeq \rho$, where ρ is the well-known FEL parameter [18]. For a good suppression, we require that the harmonics are separated by $3\sigma_\omega$, i.e.,

$$n_{\max} \simeq \frac{1}{3\rho}. \tag{8}$$

For our parameters, we have $\rho \simeq 1.7 \times 10^{-3}$ and $n_{\max} \simeq 200$.

Now let us consider the requirement that the coherent power from CHG radiator is much higher than the effective power of shot noise for the A-bunch in the amplifier. When we increase harmonic number, according to (1) we need to increase energy modulation $\Delta\mathcal{E}$ proportionally. To avoid debunching effect in CHG undulator, we need to satisfy the condition $\Delta\mathcal{E}/\mathcal{E}_0 < 1/(4N_{\rm chg})$, where $N_{\rm chg}$ is the number of periods in CHG undulator. This sets an upper limit on the radiated power, which can be calculated using the formulas from [44]. At the same time, we can estimate the effective shot noise power in the amplifier from [18]. Combining these equations, for our beam parameters we ended up with $n_{\max}$ being much higher than the one given by Eq. (8), i.e., this effect does not really limit us. This conclusion is also valid in the case when we increase uncorrelated energy spread by a factor of 3 and reduce $N_{\rm chg}$.

Another limitation may come from the requirement for the CHG radiator to be shorter than LSC debunching distance [30]. In other words, the modulated S-bunch has to radiate a sufficient amount of power before the current spikes are debunched due to LSC. Above in this paper, we mentioned that we do not expect a significant effect but it may, in principle, become a limitation if we go to much higher harmonic numbers. Combining the estimate of LSC debunching distance from [30] with formulas from [18,44], we end up again with much larger number than the one given by (8).

A peculiarity of our scheme is a low uncorrelated energy spread of the S-bunch. While the beam dynamics effects in the accelerator are complicated and difficult to predict, the energy diffusion in the modulator due to quantum fluctuations of the undulator radiation is the fundamental effect that can be easily calculated [45]. For our parameters, this effect, being added quadratically to the energy spread of the S-bunch in Fig. 7, gives 2% correction and thus can be neglected. However, if one aims at a much shorter

wavelength and has to increase electron energy, this effect must be properly taken into account with some consequences for the design of the FEL setup. The wavelength limit will then depend on the details of the design.

Another effect that can limit harmonic number in the proposed scheme is the amplification of shot noise that is proportional to the square of harmonic number [46]. We estimate signal-to-noise ratio at the laser wavelength in the modulator at 10^6. In our simulations for $n = 75$, the shot noise effect is properly included, and we did not notice any essential degradation of performance. However, for $n > 100$, we may quickly approach the situation when the FEL performance is strongly distorted due to the effect under discussion. To some extent, one can increase the laser power, but it seems unrealistic to counteract the effect at a much higher harmonic number. At the moment, we can assume that $n_{\max}$ in the range of few hundred and the wavelength around 1 nm might be a limit for this scheme if we use an ultraviolet seed laser and consider only fundamental physical effects.

We did not consider practical limitations, such as available laser power and its stability, laser phase noise, imperfections of the S-bunch and stability of its properties, and timing stability. They are specific to a given accelerator and FEL system, and the practical limit can be found experimentally. We are planning to test our scheme at FLASH up to $n \simeq 100$.

VI. CONCLUSION

We proposed two-bunch seeding concept and demonstrated its validity in start-to-end simulations. We showed that nearly Fourier-limited multigigawatt pulses can be generated at the wavelength of 4 nm in HGHG configuration with the compact undulator design of FLASH. Some aspects (EEHG case, specific matching optics, sensitivity studies, lasing at even shorter wavelengths, reduction of the required laser power at moderate harmonic numbers) will be studied in future works but already now we can conclude that the concept promises enormous improvements with respect to the traditional seeding scenarios.

ACKNOWLEDGMENTS

The authors would like to thank M. Vogt, J. Zemella, and S. Tomin for providing the optical layout shown in Fig. 3, G. Paraskaki for the help with the Genesis-1.3 simulations, and E. Ferrari for careful reading of the manuscript and useful comments. We are greatful to W. Leemans, S. Choroba, and L. Schaper for their interest in this work.

[1] E. Allaria *et al.*, The FERMI free-electron lasers, J. Synchrotron Radiat. **22**, 485 (2015).

[2] L.-H. Yu, Generation of intense UV radiation by subharmonically seeded single-pass free-electron lasers, Phys. Rev. A **44**, 5178 (1991).

[3] G. Stupakov, Using the beam-echo effect for generation of short-wavelength radiation, Phys. Rev. Lett. **102**, 074801 (2009).

[4] I. Ben-Zvi, K. M. Yang, and L. H. Yu, The "fresh-bunch" technique in FELS, Nucl. Instrum. Methods Phys. Res., Sect. A **318**, 726 (1992).

[5] D. J. Dunning, N. R. Thompson, and B. W. J. McNeil, Design study of an HHG-seeded harmonic cascade free-electron laser, J. Mod. Opt. **58**, 1362 (2011).

[6] J. Yan *et al.*, Self-amplification of coherent energy modulation in seeded free-electron lasers, Phys. Rev. Lett. **126**, 084801 (2021).

[7] G. Paraskaki *et al.*, High repetition rate seeded free electron laser with an optical klystron in high-gain harmonic generation, Phys. Rev. Accel. Beams **24**, 120701 (2021).

[8] H. Yang *et al.*, Self-enhanced coherent radiation from a free-electron laser, Fundam. Res. (2024), .

[9] E. L. Saldin, E. A. Schneidmiller, and M. V. Yurkov, Klystron instability of a relativistic electron beam in a bunch compressor, Nucl. Instrum. Methods Phys. Res., Sect. A **490**, 1 (2002).

[10] S. Heifets, G. Stupakov, and S. Krinsky, Coherent synchrotron radiation instability in a bunch compressor, Phys. Rev. ST Accel. Beams **5**, 064401 (2002).

[11] Z. Huang and K.-J. Kim, Formulas for coherent synchrotron radiation microbunching in a bunch compressor chicane, Phys. Rev. ST Accel. Beams **5**, 074401 (2002).

[12] W. Ackermann *et al.*, Operation of a free-electron laser from the extreme ultraviolet to the water window, Nat. Photonics **1**, 336 (2007).

[13] K. Tiedtke *et al.*, The soft x-ray free-electron laser FLASH at DESY: Beamlines, diagnostics and end-stations, New J. Phys. **11**, 023029 (2009).

[14] L. Schaper *et al.*, Flexible and coherent soft x-ray pulses at high repetition rate: Current research and perspectives, Appl. Sci. **11**, 9729 (2021).

[15] E. L. Saldin, E. A. Schneidmiller, and M. V. Yurkov, X-ray FEL with a meV bandwidth, Nucl. Instrum. Methods Phys. Res, Sect. A **475**, 357 (2001).

[16] Y. Ding, Z. Huang, and R. D. Ruth, Two-bunch self-seeding for narrow-bandwidth hard x-ray free-electron lasers, Phys. Rev. ST Accel. Beams **13**, 060703 (2010).

[17] Erik Hemsing, Aliaksei Halavanau, and Zhen Zhang, Enhanced self-seeding with ultrashort electron beams, Phys. Rev. Lett. **125**, 044801 (2020).

[18] E. L. Saldin, E. A. Schneidmiller, and M. V. Yurkov, *The Physics of Free Electron Lasers* (Springer-Verlag, Berlin, 2000), 10.1007/978-3-662-04066-9.

[19] F.-J. Decker *et al.*. Two bunches with ns-separation with LCLS, in *Proceedings of the 37th International Free Electron Laser Conference (FEL'15), Daejeon, Korea, 2015* (2015), WEP023, pp. 634–638, https://accelconf.web.cern.ch/FEL2015/papers/wep023.pdf.

[20] A. Marinelli *et al.*, High-intensity double-pulse x-ray free-electron laser, Nat. Commun. **6**, 2015 (2015).

[21] M. Paraliev *et al.*, SwissFEL double bunch operation, Phys. Rev. Accel. Beams **25**, 120701 (2022).

[22] A. Petralia *et al.*, Two-color radiation generated in a seeded free-electron laser with two electron beams, Phys. Rev. Lett. **115**, 014801 (2015).
[23] G. Penco *et al.*, Two-bunch operation with ns temporal separation at the FERMI FEL facility, New J. Phys. **20**, 053047 (2018).
[24] W. Decking *et al.*, A MHz-repetition-rate hard x-ray free-electron laser driven by a superconducting linear accelerator, Nat. Photonics **14**, 391 (2020).
[25] G. Penco *et al.*, Enhanced seeded free electron laser performance with a "cold" electron beam, Phys. Rev. Accel. Beams **23**, 120704 (2020).
[26] P. Rebernik Ribič, A. Abrami, L. Badano *et al.*, Coherent soft x-ray pulses from an echo-enabled harmonic generation free-electron laser, Nat. Photonics **13**, 555 (2019).
[27] D. Samoilenko *et al.*, Sensitivity of EEHG simulations to dynamic beam parameters, J. Phys. Conf. Ser. **2420**, 012024 (2023).
[28] Note that in EEHG the shot-to-shot wavelength stability is much better than in HGHG, as reported in [26].
[29] E. Hemsing, A. Marinelli, G. Marcus, and D. Xiang, Correlated energy-spread removal with space charge for high-harmonic generation, Phys. Rev. Lett. **113**, 134802 (2014).
[30] S. Khan *et al.*, Evolution of density-modulated electron beams in drift sections, Phys. Rev. Accel. Beams **27**, 040702 (2024).
[31] M. Ferrario *et al.*, Laser comb with velocity bunching: Preliminary results at SPARC, Nucl. Instrum. Methods Phys. Res., Sect. A **637**, S43 (2011).
[32] V. Petrillo *et al.*, Observation of time-domain modulation of free-electron-laser pulses by multipeaked electron-energy spectrum, Phys. Rev. Lett. **111**, 114802 (2013).
[33] J. Zemella and M. Vogt. Optics compression schemes for a possible FLASH upgrade, in *Proceedings of the 10th International Particle Accelerator Conference (IPAC), Melbourne, Australia* (2019), p. 1744, https://accelconf.web.cern.ch/ipac2019/doi/JACoW-IPAC2019-TUPRB026.html.
[34] The laser heater at FLASH uses the originally proposed layout [35] with the undulator on the straight path and a chicane in front of it for in-coupling of the laser radiation.
[35] E. L. Saldin, E. A. Schneidmiller, and M. V. Yurkov, Longitudinal space charge-driven microbunching instability in the TESLA Test Facility linac, Nucl. Instrum. Methods Phys. Res., Sect. A **528**, 355 (2004).
[36] K. Floettmann, *ASTRA: A Space Charge Tracking Algorithm* (DESY, 2017).
[37] I. Zagorodnov and M. Dohlus, Semianalytical modeling of multistage bunch compression with collective effects, Phys. Rev. ST Accel. Beams **14**, 014403 (2011).
[38] S. Tomin, I. Agapov, M. Dohlus, and I. Zagorodnov, Ocelot as a framework for beam dynamics simulations of x-ray sources, in *Proceedings of the International Particle Accelerator Conference (IPAC), Copenhagen, Denmark* (2017), WEPAB031.
[39] I. Zagorodnov, M. Dohlus, and S. Tomin, Accelerator beam dynamics at the european X-ray free-electron laser, Phys. Rev. Accel. Beams **22**, 024401 (2019).
[40] I. Zagorodnov, S. Tomin, Y. Chen, and F. Brinker, Experimental validation of collective effects modeling at injector section of x-ray free-electron laser, Nucl. Instrum. Methods Phys. Res., Sect. A **995**, 165111 (2021).
[41] I. Zagorodnov and T. Weiland, TE/TM field solver for particle beam simulations without numerical Cherenkov radiation, Phys. Rev. ST Accel. Beams **8**, 042001 (2005).
[42] C. Lechner, M. Dohlus, B. Faatz, V. Grattoni, G. Paraskaki, J. Rönsch-Schulenburg, E. Schneidmiller, M. Yurkov, and J. Zemella, Experimental test of longitudinal space-charge amplifier in optical range, in *Proceedings of 10th International Particle Accelerator Conference, Melbourne, Australia* (2019), p. 3267, 10.18429/JACoW-IPAC2019-WEPTS061.
[43] S. Reiche, Genesis 1.3: A fully 3D time-dependent FEL simulation code, Nucl. Instrum. Methods Phys. Res., Sect. A **429**, 243 (1999).
[44] E. L. Saldin, E. A. Schneidmiller, and M. V. Yurkov, A simple method for the determination of the structure of ultrashort relativistic electron bunches, Nucl. Instrum. Methods Phys. Res., Sect. A **539**, 499 (2005).
[45] E. L. Saldin, E. A. Schneidmiller, and M. V. Yurkov, Calculation of energy diffusion in an electron beam due to quantum fluctuations of undulator radiation, Nucl. Instrum. Methods Phys. Res., Sect. A **381**, 545 (1996).
[46] E. L. Saldin, E. A. Schneidmiller, and M. V. Yurkov, Study of a noise degradation of amplification process in a multistage HGHG FEL, Opt. Commun. **202**, 169 (2002).